Reduced gravity and muon radiation affect *Caenorhabditis elegans* life history traits and viral infection

Ana Villena-Giménez,[1] Victoria G. Castiglioni[1], Juan C. Muñoz-Sánchez,[1,2], Esmeralda G. Legarda[1], Rubén González[3], Santiago F. Elena[1,4]

[1]Instituto de Biología Integrativa de Sistemas (CSIC-UV), Paterna, 46980 Valencia, Spain
[2]Department of Theoretical Physics, Universitat de València, Burjassot, 46100 Valencia, Spain
[3]Institute Pasteur, 75015 Paris, France
[4]Santa Fe Institute, Santa Fe, NM 87501, USA

Correspondence: santiago.elena@csic.es

ORCIDs:
A.V-G.: 0009-0000-3564-4293
V.G.C.: 0000-0001-9884-2537
J.C.M-S.: 0000-0002-5570-4983
E.G.L.: 0000-0002-8560-8407
R.G.: 0000-0001-9588-1127
S.F.E.: 0000-0001-8249-5593

ABSTRACT

Conditions beyond Earth —including gravitational forces and radiation exposure— often deviate substantially from those at the planet's surface. In this study, we investigated the effects of reduced gravity (simulated through a Random Positioning Machine) and below-background radiation (primarily lowered muon flux in an underground facility) on Orsay virus infection in the nematode *Caenorhabditis elegans*. We employed a fully factorial experimental design, examining how each factor, alone and in combination, influences physiological traits and viral load. While below-background radiation increased viral accumulation, reduced gravity tended to decrease it. Both factors significantly impacted reproduction and morphology, with some effects magnified by viral infection. These results reveal how partial modifications of Earth-like gravity and radiation levels can alter pathogen–host interactions. Although this work does not encompass the full complexity of space environments —where cosmic radiation includes high-energy protons and heavy ions— it provides insight into how adjustable models of reduced gravity and radiation can advance our understanding of biological adaptation beyond standard terrestrial conditions.

INTRODUCTION

Organisms in off-Earth environments may experience a variety of unusual stresses, including reduced gravitational forces (microgravity, μG) and substantial changes in radiation exposure. These perturbations can affect overall health and immunity. For instance, within relatively short-duration orbital missions (between 10 and 15 days), blood samples from astronauts showed altered levels of leukocyte distribution and cytokine production and a decrease in the function of Epstein-Barr virus specific $CD8^+$ T cells[1]. During longer missions (6 months), immune alterations persisted, as evidenced by reduced T-cell function[2], impairment of natural killer cells function[3] and elevated levels of salivary antimicrobial proteins[4]. Indeed, the reactivation of latent herpesviruses is well documented in astronauts[4-6]: Epstein-Barr virus, varicella-zoster virus and cytomegalovirus infections increased in frequency, duration and amplitude the longer the duration of space missions[5,7].

Radiation composition in off-Earth settings differs substantially from that on Earth's surface. One of the radiation components that differs between space and Earth's surface is the muon —a charged elementary particle produced when pions decay following cosmic ray interactions with atmospheric molecules. Muons are the main cosmic radiation at sea level, with about 600 muons crossing a human body every minute[8]. As an important source of radiation for living beings, cells have developed mechanisms that buffer muon's detrimental effects[9,10]. This observation is relevant to radiation hormesis, in which organisms may benefit from low-level radiation exposure but experience detrimental effects when doses deviate significantly in either direction[11].

Caenorhabidits elegans has long served as a valuable model for studying diverse stresses that can be challenging to dissect in more complex animals. *C. elegans* is a well-characterized metazoan that has been widely employed since its introduction by Sydney Brenner in the 1970s[12]. As a model organism, it has many advantages: easy visualization, fast development, a complete characterized cell lineage and genome, and an estimated genetic homology of ~80% of the protein-coding genome with humans[13]. *C. elegans* is exposed to fluctuating environmental conditions in its natural environment, such as heat, cold, food scarcity, oxygen levels, and osmotic perturbations. While repeated mild heat-shock treatments extend *C. elegans* lifespan[14], moderate treatments impair fecundity[15] and embryogenesis[16], and severe treatments decreases longevity[17]. These heat-shock phenotypic alterations are synchronized with a strong change in the transcriptional response[18]. Exposure to other abiotic stresses, such as hypertonic environments induce transcriptional responses that mimic infection response to a variety of pathogens[19] and heat shocked animals have increased survival upon exposure to *Staphylococcus aureus*[20]. In contrast, animals fed with pathogenic bacteria[21] or infected with virus[22] show an increased resistance to heat shock and ubiquitin ligases involved in the intracellular pathogen response (IPR) promote thermotolerance in order to cope with proteotoxic stress, unveiling the close link between biotic and abiotic stresses[23].

C. elegans has long been used as a model in immunity. It can regulate immune responses recognizing pathogens, influencing the body's development, and controlling avoidance behavior[24]. Although there are significant differences with the immune system of mammals, some mechanisms used to limit pathogenesis show remarkable phylogenetic conservation, such as uridylation and RNAi pathways[25,26]. Since the discovery of Orsay virus (OrV), a lot of effort has been put into the characterization of virus-host interaction dynamics. OrV is a bipartite positive-sense single-stranded RNA virus related to the *Nodaviridae* family that infects *C. elegans* intestinal cells[27]. Viral infection produces mild intestinal symptoms such as changes in cytoplasm viscosity, nuclear degeneration and cellular fusion[27], while mild effects in progeny production where only observed in a more susceptible strain[26]. Links between viral infection and abiotic stresses have been described in the nematode, with heat stress reducing its susceptibility to OrV[28] and, conversely, OrV-infected animals showing an increased tolerance to heat-shock[22].

Finally, the effect of below background radiation (BBR) environments and μG on *C. elegans* and other model organisms has been explored before. Van Voorhies *et al*. carried out phenotypic and transcriptomic studies in *C. elegans* at the underground laboratory at the Waste Isolation Pilot Plant (New Mexico, USA)[29]. Animals had faster larval growth rates, higher egg laying rates and a different gene expression profile, both at 72 h after being at BBR and after 10 generations[29]. Moreover, a reduction in fertility has been observed in *Drosophila melanogaster* flies reared at the Gran Sasso Underground laboratory (Italy)[30]. Studies in simulated μG conditions in *C.*

elegans have reported no reproductive and lifespan changes in nematodes[31], increased intestinal barrier permeability[32] and induction of oxidative stress and dysregulated antioxidant machinery[33].

In this study, we have explored the role of two off-Earth stresses, μG and BBR, on the outcome of a viral infection. To do so, we have studied the *C. elegans*/OrV pathosystem under a factorial combination of two abiotic factors: gravity intensity (standard and μG) and muon radiation flux (standard and BBR). We acclimatized the host to the abiotic stresses and performed the experiments in the third generation of acclimatized animals. This enabled us to investigate long-term effects of μG and BBR in the nematode since it is known that in *C. elegans* responses to stress are transmitted intergenerationally[32]. We have measured different fertility traits as a proxy to the animal's fitness, and body length and morphology to identify developmental impairments. We also assessed intestinal barrier permeability to determine the functional state of the intestine under these stresses, since OrV infects intestinal cells and intestinal collagens are involved in preventing viral entry[34]. In addition, we quantified OrV genomic RNA2 accumulation as a proxy to viral fitness under these different stress conditions. Finally, the data was fitted to a fertility model and different parameters associated to prezygotic (early oocyte development, maturation and fertilization rates) and postzygotic (abortion rate) effects estimated.

RESULTS

The impairment of intestinal barrier by μG is antagonized by BBR

Intestinal integrity is critical for overall health[35], as it is key to nutrient absorption and serves as a primary defense against enteric pathogens —including OrV. Previous work has shown that various abiotic stresses can alter intestinal permeability, with microgravity (μG) in particular causing a significant increase[31]. Accordingly, we sought to validate our simulated microgravity conditions by determining whether they recapitulate this known phenotype. Additionally, we examined how reduced background radiation (via lowered muon flux) might counterbalance or compound these effects. To measure gut permeability, we employed a dye-based assay in which worms are exposed to a blue dye. An intact intestinal barrier restricts the dye to the lumen; conversely, compromised integrity leads to dye leakage into surrounding tissues (Fig. 1a). Firstly, we observed a large and significant overall increase in permeability of animals grown in μG conditions ($\chi^2 = 15.882$, 1 d.f., $P < 0.001$, $\eta_P^2 = 0.187$), as previously reported. Conversely, BBR conditions were associated to a moderate but still significant reduction in permeability ($\chi^2 = 8.387$, 1 d.f., $P = 0.004$, $\eta_P^2 = 0.099$). No significant interaction between the two factors has been found ($\chi^2 = 0.461$, 1 d.f., $P = 0.497$), suggesting that permeability alterations are a consequence of overlapping mechanisms (Fig. 1b).

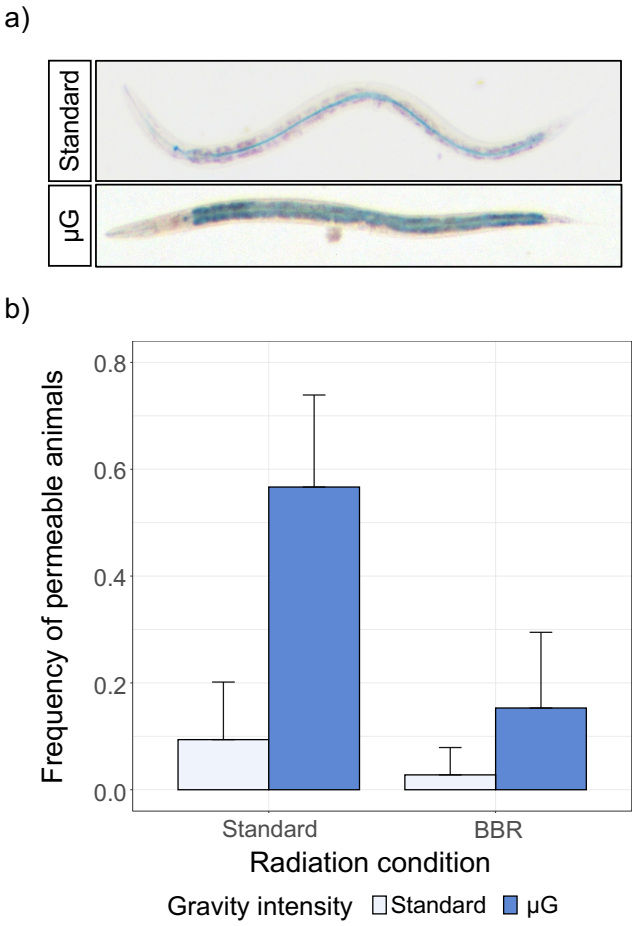

Figure 1. (a) Representative animals in standard (non-permeable) and µG conditions (impaired permeability). Nematodes showing blue staining outside the intestinal tube were scored as permeable whether the salt diffused throughout the body out. **(b)** Intestinal permeability of animals under standard gravity (n = 30), µG (n = 28), BBR (n = 34) and µG plus BBR (n = 24) conditions. Synchronized L1 animals were grown at 20 ºC during 48 h and then fed with a solution containing erioglaucine disodium for 3 h. Error bars represent ±1 SEM.

Viral accumulation dynamics are affected by gravity and radiation intensity

Having confirmed that our simulated conditions produced the expected phenotypic changes in *C. elegans* (for instance, increased intestinal permeability under reduced gravity), we next examined whether viral infections remained successful under these modified environments. Our laboratory has previously demonstrated that, under standard laboratory conditions (*i.e.*, Earth-like gravity and muon radiation flux), OrV infection in *C. elegans* follows two waves of viral load from L1 larvae to sexually mature adults[36]. A first peak is reached approximately 12 hours post-inoculation (hpi) in L1 larvae, which is followed by a sharp decline as antiviral responses are activated by the developing animals, reaching a minimum approximately 18 – 20 hpi (L2 larvae). From there on, a second wider peak is reached that last for at least 18 additional hours (L3 larvae and L4), afterwards, viral load is low, yet viral replication continues at low levels[36]. In this work, we

observed that under our standard reference conditions, OrV likewise exhibited these two distinct waves, thus confirming the reproducibility of its infection dynamics (Fig. 2, upper left panel). We then asked whether reducing gravity and muon flux would alter either the timing or amplitude of these phases.

Gravity intensity and muon radiation flux conditions had effects of opposite sign on viral load dynamics. The grand mean viral load measured in μG conditions was $(5.69 \pm 0.05)\cdot 10^4$, lower than the $(2.53 \pm 0.02)\cdot 10^5$ in standard gravity conditions, representing a small yet significant effect ($\chi^2 = 2255.942$, 1 d.f., $P < 0.001$; $\eta_P^2 = 0.058$). As illustrated in Fig. 2, the net effect of μG is time-dependent ($\chi^2 = 1415.456$, 19 d.f., $P < 0.001$; $\eta_P^2 = 0.037$) and, averaging across muon flux radiation conditions, consists in reducing the height of the first peak of viral load and increasing the maximum value and duration of the second (both left *vs* both right panels in Fig. 2). The grand mean viral load measured in BBR conditions (averaging both lower panels in Fig. 2) was $(1.87 \pm 0.02)\cdot 10^5$, compared to a value of $(7.67 \pm 0.06)\cdot 10^4$ measured in normal muon radiation flux conditions (averaging both upper panels in Fig. 4), representing a major increase in viral load ($\chi^2 = 1593.430$, 1 d.f., $P < 0.001$; $\eta_P^2 = 0.041$). The effect of BBR widely impact the temporal dynamics of OrV accumulation ($\chi^2 = 3103.138$, 19 d.f., $P < 0.001$; $\eta_P^2 = 0.080$), erasing the differences between the two peaks, as only a maximum value is reached about 12 hpi that remains constant until 36 hpi and then slowly declines (upper *vs* lower left panels in Fig. 2).

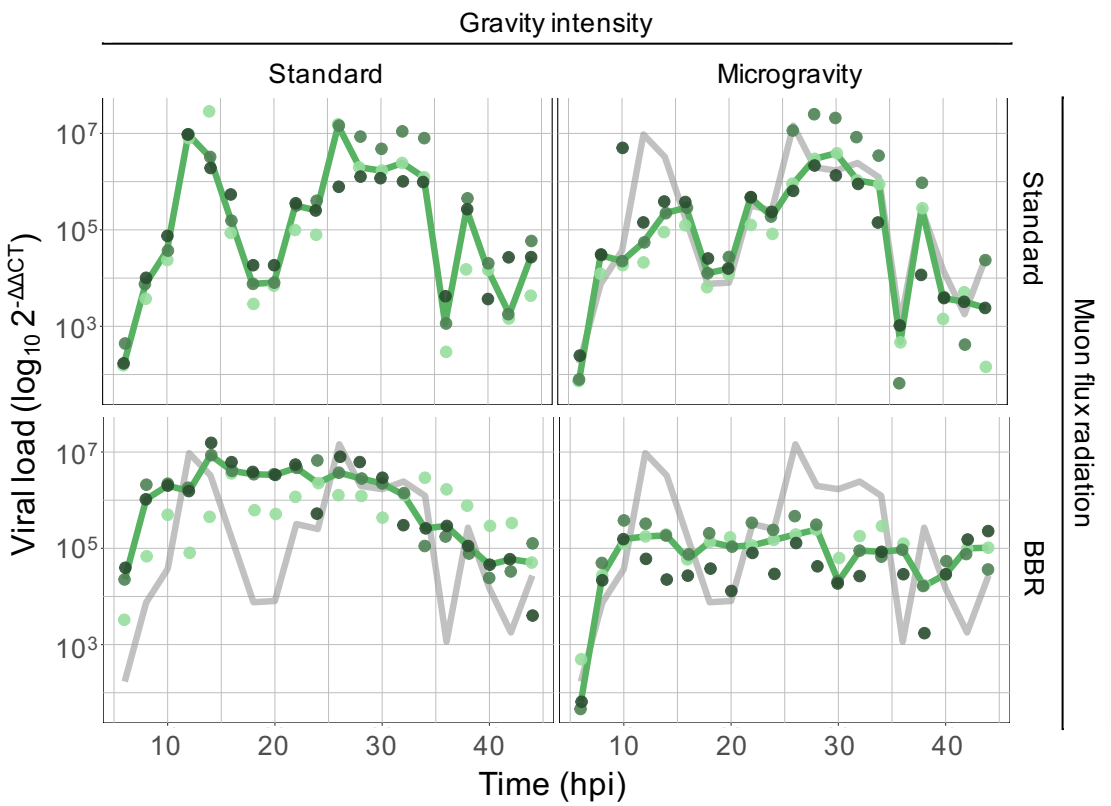

Figure 2. Log-fold change of OrV accumulation, relative to the expression of housekeeping gene *cdc-42*, evaluated in inoculated animals reared under the indicated combination of gravity intensity and muon radiation flux conditions. Different green tones represent independent biological replicates (pools of ~300 animals per time point). The solid green lines represent the median trajectory. For the sake of comparison, the gray solid lines represent the OrV dynamics observed in standard laboratory conditions.

The observed effects were not independent, as a significant interaction term has been found among them (χ^2 = 1636.075, 1 d.f., $P < 0.001$; $\eta_P^2 = 0.042$) that was also time-dependent (χ^2 = 1934.595, 19 d.f., $P < 0.001$; $\eta_P^2 = 0.050$). The combined effect of both environmental stresses in viral fitness shows the atypical pattern observed in BBR conditions but with a further reduction in viral load along the whole period of animal development (upper left *vs* lower right panels in Fig. 2).

Overall, μG has a negative impact on viral replication, whilst BBR has a positive one and the combination of these stresses has an even greater negative impact than by themselves.

Fecundity traits are affected by reduced gravity and radiation

OrV infections are typically described as having only a mild impact on *C. elegans* fitness[37]. To determine whether this impact might be altered by our environmental treatments, we performed time-series measurements of three fecundity-related traits —number of viable progeny (A), number of unfertilized eggs (U), and number of nonviable embryos (N)— in four conditions: standard environment, μG, BBR, and the combination of μG plus BBR (Fig. S1). These measurements were done both in non-inoculated animals (control; blue lines and circles) and in OrV-inoculated ones (OrV; green lines and triangles). All these data were fitted to the generalized linear mixed model (GLMM) described in the Methods section. The results from these analyses are shown in Table 1. For a detailed description of the effect of the different stresses on A, U and N, we refer to the supplementary text in Supplementary Materials online. Here, we will focus on the combination of these three traits into a more eco-evolutionary relevant trait, the per day reproductive success defined as $R(t) = A(t)/[A(t) + N(t) + U(t)]$ (Fig. 3). Focusing first on the effects of the environmental conditions in non-inoculated animals, we found that differences in gravity intensity had a significant effect, though of small magnitude (Table 1; $P < 0.001$, $\eta_P^2 = 0.022$), with animals reared at standard gravity having an average R of 0.950 ±0.005 that was reduced to 0.927 ±0.004 in μG. The effect of muon radiation flux was conditional to the value of gravity intensity (Table 1; $P = 0.002$, $\eta_P^2 = 0.016$). In μG, R was not affected by differences in muon radiation flux (*post hoc* test, $P = 0.691$). However, in standard gravity conditions the quasi-

elimination of muon radiation flux was associated with a reduction in average R from 0.962 ±0.007 to 0.939 ±0.006 (*post hoc* test, $P < 0.001$).

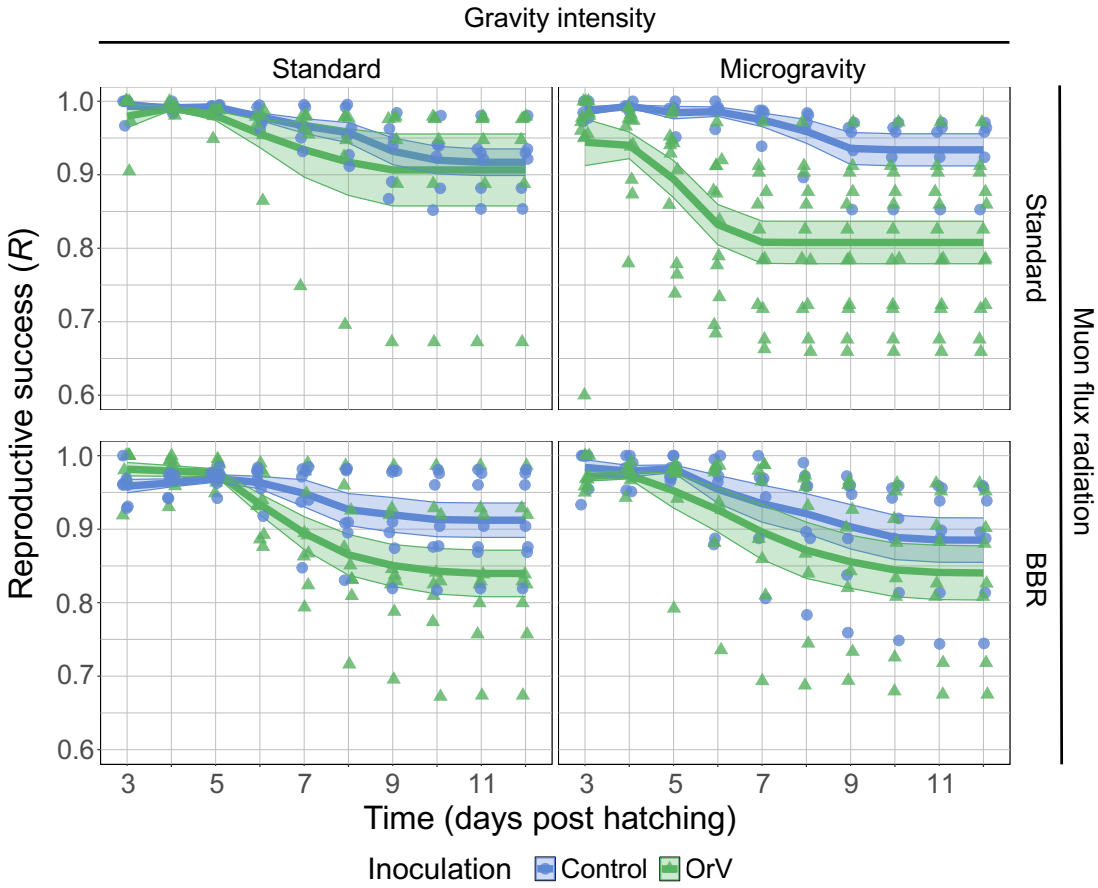

Figure 3. Per day reproductive success (R) of OrV-inoculated (green) and non-inoculated (blue) animals under different combinations of environmental stresses. Color triangles and circles represent replicates and solid lines the mean of replicates with ±1 SEM plotted as a ribbon. Number of non-inoculated animals: $n = 6$ for standard conditions, $n = 5$ for μG, $n = 7$ for BBR, and $n = 7$ for μG and BBR. Number of inoculated animals: $n = 6$ for standard conditions, $n = 12$ for μG, $n = 9$ for BBR, and $n = 8$ for BBR plus μG.

R was also negatively affected by infection itself (Table 1; $P < 0.001$, $\eta_P^2 = 0.074$), with inoculated animals having grand mean R of 0.917 ±0.004 and non-inoculated animals of 0.961 ±0.005, an effect of moderate magnitude. The effect of inoculation was mediated by gravity intensity (Table 1; $P < 0.001$, $\eta_P^2 = 0.024$). While R for non-inoculated animals was indistinguishable for both gravity conditions (0.960 ±0.006 in standard *vs* 0.961 ±0.007 in μG; *post hoc* test, $P = 0.889$), the mean R of inoculated animals exposed to μG was significantly lower (0.894 ±0.005 *vs* 0.941 ±0.006 in standard gravity; *post hoc* test, $P < 0.001$). The effect of inoculation was also mediated by the muon radiation flux (Table 1; $P = 0.004$, $\eta_P^2 = 0.014$). In

202 this case, R of non-inoculated animals was significantly smaller in BBR conditions than in
203 standard ones (0.949 ±0.006 *vs* 0.972 ±0.007; *post hoc* test, P = 0.020), while no effect was
204 observed for inoculated animals (0.924 ±0.006 *vs* 0.910 ±0.006; *post hoc* test, P = 0.088). Finally,
205 the effect of inoculation significantly depended on the interaction between the two environmental
206 conditions (Table 1; $P < 0.001$, $\eta_P^2 = 0.018$). The largest effect on R was observed for inoculated
207 animals grown under μG and standard muon radiation flux (0.866 ±0.007), while the smallest
208 effect was seen for non-inoculated animals under the same combination of factors (0.97 ±0.01).
209 In conclusion, both off-Earth conditions impacted reproductive success, though their effects
210 varied across traits. μG reduced reproductive success. BBR reduced reproductive success in
211 standard gravity, and its effects were smaller or absent in μG. In standard conditions, OrV
212 negatively impacted the animals' reproductive success, especially by increasing the number of
213 unfertilized eggs. These effects are worsened by μG but somewhat buffered by BBR, indicating
214 that these stresses likely affect different pathways of the infection response.
215
216 **The observed effects of BBR and viral infection are prezygotic**
217 The above statistical descriptions and analyses highlight the effect of the three experimental
218 factors in the data. However, this sort of analyses fails to provide a mechanistic explanation for
219 the observed differences. To dig into possible mechanisms, we developed a simple model that
220 describes the processes from the maturation of germline precursors up to the hatching of eggs to
221 liberate L1 larvae. The model is described by the set of six ordinary differential equations given
222 by Eqs. 1 – 6 (see Methods). The model includes five parameters to describe different processes.
223 Fitting the data shown in Fig. 1 into Eqs. 1 – 6 allows to disentangle whether observed differences
224 in A, N and U under different environments and infection status can be attributable to pre- or post-
225 zygotic effects. Table 2 shows the fitting estimates for each condition (see Fig. S2 for illustration
226 of the best fittings). Table S1 shows the results of the three-ways ANOVA model fitted to the
227 parameter estimates. Gravity intensity itself had no significant effect on any of the six model
228 parameters. Muon radiation flux had significant effects, of large magnitude, in the rates of
229 germline precursors differentiation into mature oocytes (δ) as well as in the rate of oocyte
230 migration from the gonads into the spermathecae (η). Animals reared in BBR conditions
231 experienced a reduction in both parameters, in the case of δ from 0.65 ±0.03 d^{-1} to 0.45 ±0.02 d^{-1}
232 (*post hoc* test $P < 0.001$); in the case of η from 0.92 ±0.06 d^{-1} to 0.69 ±0.06 d^{-1} (*post hoc* test P
233 = 0.008).
234 Infection status had a significant effect of large magnitude in δ and η (Table S1; $P < 0.001$, η_P^2
235 ≥ 0.209 in both cases) and significant but of moderate magnitude in the initial number of germline
236 precursors (G_0) and in spermatocyte to germline precursors initial ratio (α) (Table S1; $P \leq 0.038$,
237 $\eta_P^2 \leq 0.107$ in both cases). Inoculated animals show a reduction in δ from 0.62 ±0.03 d^{-1} to 0.47

±0.02 d^{-1} (*post hoc* test $P < 0.001$), an increase in η from 0.65 ±0.06 d^{-1} to 0.96 ±0.06 d^{-1} (*post hoc* test $P < 0.001$), a reduction in α from 0.92 ±0.02 to 0.86 ±0.02 (*post hoc* test $P = 0.016$), and an increase in G_0 from 270 ±14 to 309 ±12 (*post hoc* test $P = 0.038$).

Table S1 also shows that some of the effects involved interactions between the three environmental factors. Firstly, δ was affected by gravity intensity in a manner dependent on the muon radiation flux (significant interaction gravity by radiation term; $P = 0.006$, $\eta_P^2 = 0.138$): in standard muon radiation flux and standard gravity $\delta = 0.72 \pm 0.04$ d^{-1}, but reduced to $\delta = 0.58 \pm 0.03$ d^{-1} in μG (19.7% reduction; *post hoc* test $P = 0.003$); in BBR conditions and standard gravity $\delta = 0.42 \pm 0.03$ h^{-1}, statistically undistinguishable from $\delta = 0.47 \pm 0.03$ d^{-1} in μG (*post hoc* test $P = 0.107$). Secondly, the magnitude of the effect of muon radiation flux on δ and η also depended on the infection status (Table S1; $P \leq 0.001$, $\eta_P^2 \geq 0.188$ in both cases). In the case of δ, non-inoculated animals reared in standard muon radiation flux conditions had $\delta = 0.78 \pm 0.04$ d^{-1}, while at BBR conditions, $\delta = 0.46 \pm 0.03$ d^{-1}, representing a significant reduction (*post hoc* test $P < 0.001$); inoculated animals grown at standard muon radiation flux conditions had $\delta = 0.51 \pm 0.03$ d^{-1}, while at BBR conditions, $\delta = 0.43 \pm 0.03$ d^{-1}, representing a significant reduction (*post hoc* test $P = 0.036$). In other words, the magnitude of the effect on δ due to muon radiation flux was larger in non-inoculated animals than in inoculated ones (41.6% *vs*. 15.56% reductions). In the case of η, non-inoculated animals reared in standard muon radiation flux had $\eta = 0.6 \pm 0.1$ d^{-1}, while at BBR conditions, $\eta = 0.68 \pm 0.08$ d^{-1}, values that were not significantly different (*post hoc* test $P = 0.315$); inoculated animals grown at standard muon radiation flux conditions had $\eta = 1.22 \pm 0.08$ d^{-1}, while at BBR conditions, $\eta = 0.70 \pm 0.08$ d^{-1}, representing a significant reduction (*post hoc* test $P < 0.001$). In other words, the magnitude of the effect on η due to muon radiation flux was larger in inoculated animals than in non-inoculated ones (44.0% reduction *vs*. 9.8% nonsignificant increase).

In conclusion, we found that the three environmental factors had significant effects in parameters related to prezygotic processes, with the magnitude and sign of the observed changes depending on the precise combination of factors. In terms of wider effects, OrV infection affected more developmental processes than either muon radiation flux or gravity intensity.

Synergistic effects of μG, BBR and infection in developmental rates

To better understand the effects of these environmental factors in another key developmental/health metric, we next focused on larval development (Fig. 4a). There was a significant overall effect of gravitational differences yet of small magnitude ($\chi^2 = 45.734$, 1 d.f., $P < 0.001$, $\eta_P^2 = 0.005$), with animals raised in μG being larger than those raised under standard conditions (grand mean values: 678 ±4 μm *vs* 640 ±4 μm). Furthermore, the difference is size

increased with time post-hatching (χ^2 = 48.942, 3 d.f., P < 0.001; η_P^2 = 0.006). Muon radiation flux also had a significant overall effect of small magnitude (χ^2 = 28.179, 1 d.f., P < 0.001, η_P^2 = 0.003), with nematodes exposed to BBR conditions being larger than those in standard conditions (674 ±4 μm *vs* 644 ±4 μm). The effect magnitude was also time-dependent (χ^2 = 17.747, 3 d.f., P < 0.001; η_P^2 = 0.002). Inoculation had a significant impact as well (χ^2 = 20.630, 1 d.f., P < 0.001, η_P^2 = 0.002), with inoculated animals being smaller than their non-inoculated counterparts (647 ±4 μm *vs* 672 ±4 μm). The effect magnitude varied over time, generally increasing (χ^2 = 14.983, 3 d.f., P = 0.002; η_P^2 = 0.002), though not uniformly across all conditions.

The magnitude of these effects depended on the pairwise interactions of the three factors (χ^2 ≥ 10.424, 1 d.f., P ≤ 0.001, η_P^2 ≤ 0.003 in all combinations) and varied over time (χ^2 ≥ 12.269, 3 d.f., P ≤ 0.007, η_P^2 ≤ 0.002 in all combinations). Focusing first in the interaction between gravity intensity and muon radiation flux, animals grown in μG under BBR conditions were, on average, larger than those grown only in μG (702 ±6 μm *vs* 654 ±5 μm; *post hoc* test, P < 0.001) and larger than those grown only under BBR conditions (702 ±6 μm *vs* 646 ±6 μm; *post hoc* test, P < 0.001). Now looking at the interaction between gravity intensity and inoculation, we found that under standard gravity intensity, inoculated animals were on average smaller than non-inoculated ones (618 ±6 μm *vs* 671 ±4 μm; *post hoc* test, P < 0.001), while inoculation had no significant effect on growth under μG conditions (675 ±6 μm *vs* 673 ±6 μm; *post hoc* test, P = 0.602). Finally, exploring the interaction between muon radiation flux and inoculation, we observed that inoculation had no net effect on animals grown under BBR conditions (675 ±6 μm *vs* 673 ±6 μm; *post hoc* test, P = 1). Three-way interactions were not statistically significant either independently (χ^2 = 0.225, 1 d.f., P = 0.636) or over developmental time (χ^2 = 2.034, 3 d.f., P = 0.565), indicating that the effect of infection was independent on the interaction between the two abiotic stresses.

Populations of *C. elegans* are typically dominated by hermaphrodites, with males arising infrequently under standard conditions —only once per 1606 individuals in our experiments. Although rare, males can be biologically significant by enabling outcrossing, which increases genetic diversity and may facilitate adaptation under stressful conditions[38]. Notably, the frequency of males increased when worms were subjected to reduced gravity or BBR. For instance, we found four males in a population of 733 under μG, 15 out of 3490 under BBR alone, and five out of 1640 under combined μG and BBR (Fig. 4b). While neither gravity intensity (χ^2 = 2.606, 1 d.f., P = 0.106) nor muon ration flux (χ^2 = 1.431, 1 d.f., P = 0.232) alone significantly affected the number of males produced, their combination led to a ~5-fold increase in male frequency compared to standard conditions, a statistically significant yet small effect (χ^2 = 5.315, 1 d.f., P = 0.021, η_P^2 = 0.001).

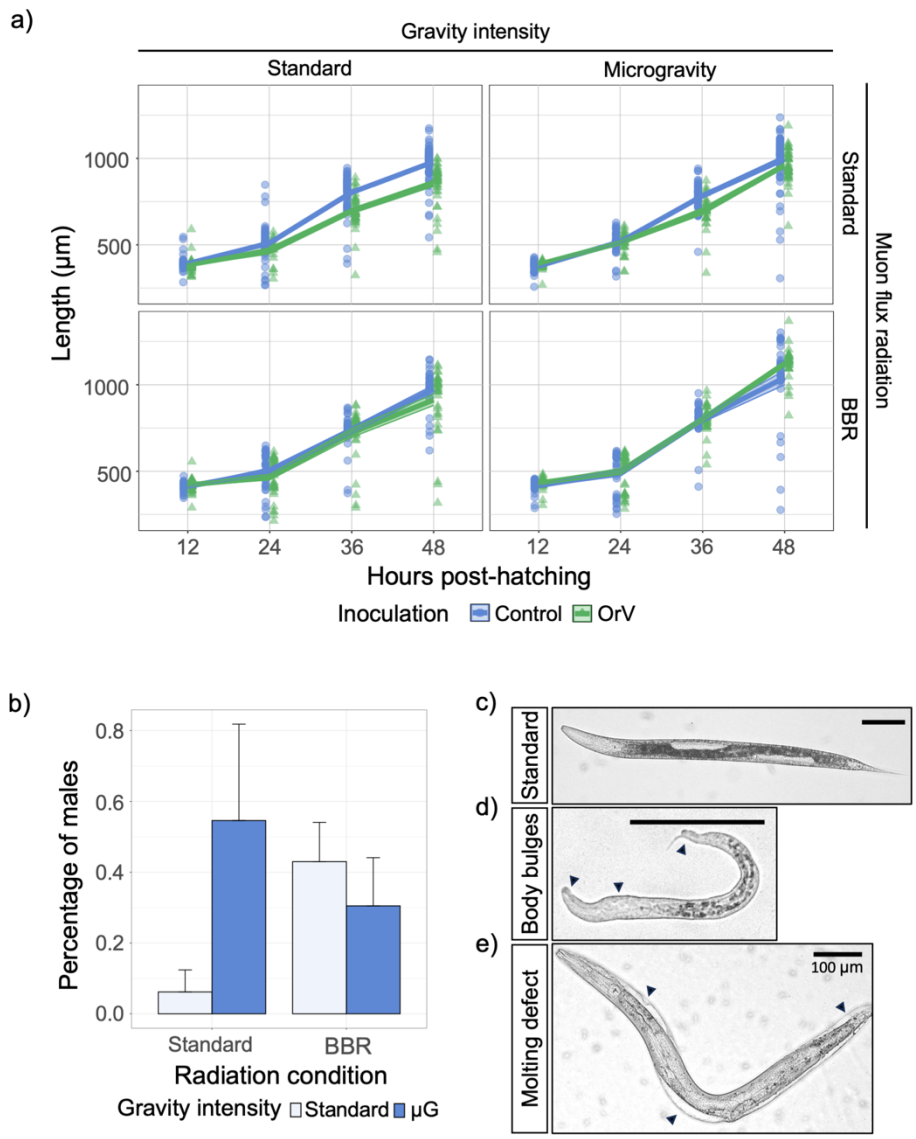

Figure 4. Growth and development of non-inoculated and OrV-inoculated animals under different gravity and radiation conditions. (**a**) Starting from plates with 400 individuals, photographs were taken at 12, 24, 36, and 48 hours after hatching to assess the effect of the stress conditions in larval development. Solid lines represent the mean and ribbons represent ±1 SEM (number of replicates ranged from 19 to 130). (**b**) Percentage of males quantified 48 h after hatching under standard (n = 1606), µG (n = 733), BBR (n = 3490), and BBR plus µG (n = 1640). Error bars represent ±1 SEM. (**c**) Animal grown in standard conditions. **(d)** Individual with bulges around the body and short length. Extracted from the population of 24 h in BBR conditions; scale bar of 100 µm. (**e**) Individual defective in molting. Extracted from the population 48 h in BBR plus µG; scale bar of 100 µm.

In addition, under BBR conditions we observed dumpy animals —characterized by a shorter and stouter body morphology due to defects in structural genes like collagens (3 in a population of 1843 individuals), as well as other phenotypes that deviate from the standard (Fig. 4c), which

312 included increased head-length proportion, body bulges (Fig. 4d) and molting defects (Fig. 4e).
313 Neither of these phenotypes were observed in standard conditions (Binomial test, $P < 0.001$). A
314 possible explanation is that lack of radiation might affect genes that are involved in molting, such
315 as collagens[39].
316 In conclusion, OrV inoculation mitigates the effect of the two abiotic stresses on
317 developmental rates, the two abiotic stresses result in increased male frequency and BBR also
318 causes diverse morphological abnormalities.
319
320
321 **DISCUSSION**
322 In this study, we sought to investigate the independent and combined effects of two off-Earth
323 environmental factors —reduced gravity and absence of muon radiation flux— on a biological
324 system comprising *C. elegans* and its natural viral pathogen OrV. Previous work suggested that
325 even partial modifications of Earth-like gravity and radiation levels could influence immune
326 responses and pathogen–host interactions[7,40,41]. Consequently, we focused primarily on reduced
327 muon flux (the major component of cosmic radiation at sea level) in an underground laboratory,
328 and on simulated reduced gravity using a Random Positioning Machine (RPM). Whilst these
329 conditions explore only a subset of the large spectrum of off-Earth stresses (which also include
330 heavy-ion radiation, solar particle events, and near-vacuum states[42]), our results nonetheless
331 provide insight into how each stressor, alone and in combination, can impact viral infection and
332 animal physiology.
333 Our first goal was to validate that our reduced-gravity simulation on agar plates recapitulated
334 previously reported phenotypes, such as increased intestinal permeability under microgravity[32].
335 Although agar plate-based RPM experiments do not fully mimic true weightlessness, and surface
336 tension can interfere with microgravity simulation fidelity[43], we still observed a significant
337 compromise in intestinal integrity under μG. Furthermore, RPM microgravity simulation in agar
338 plates has been proved to induce changes in *C. elegans* physiology[31], while liquid culture in a
339 RPM produces a shear stress that should be acknowledged[44]. It is also worth-mentioning that
340 liquid culture in *C. elegans* has an impact in gene expression[45] and growth[46], which represents a
341 disadvantage when considering other microgravity simulation systems. Conversely, culturing
342 worms under BBR (*i.e.*, drastically reduced muon flux) partially offset these μG-induced effects,
343 suggesting that microgravity and BBR elicit overlapping but distinct physiological responses.
344 Our results confirm previous observations that both μG and BBR represent stressful
345 environments that affect responses to viral infections[1-7] and developmental rates and fecundity[29].
346 Interestingly, our data show that the magnitude of these effects varied for different fecundity
347 components and developmental rates, and that the two environmental stresses acted non-

348 independently. This non-independence of effects suggests that the animal's responses to μG and
349 BBR should at least partially overlap.
350 The small but significant increase in male frequency in the combination of the two stresses
351 suggests that off-Earth conditions may disrupt cellular homeostasis and processes as important as
352 chromosomal disjunction could be affected by these stresses, as has been observed with other
353 environmental stresses[47]. Furthermore, increasing the number of males could have big
354 consequences at the population level, as increased mating increases genetic diversity in the
355 population by promoting allele shuffling and thus bolstering adaptation to the stressful
356 conditions[38,48].
357 Larval development, measured as body length, was also affected by the two off-Earth
358 conditions. Animals grown under μG or BBR conditions are larger, and their combination
359 resulted in a further increase in body length. The μG results are in disagreement with previous
360 works, which reported decreased body length in simulated microgravity[33] and in spaceflight[49].
361 This difference is probably due to experimental design, as our animals were preadapted to the μG
362 environment during two generations, grew on solid medium, and the start point and duration of
363 μG exposure were different, and were not subjected to any other environmental stress such as
364 synchronization by bleaching or spaceflight, which encompass a wide variety of stresses that can
365 account for the difference in body length in comparison with our results. Regarding viral
366 infection, OrV inoculated animals in standard conditions were shorter than non-inoculated, while
367 it had no effect when other stresses are applied. This is the first time that an effect of OrV infection
368 in development is described, as *C. elegans* has not been a model to study virus-host interactions
369 until recently. Body size in adults was described to be decreased in adult animals expressing
370 human hepatitis delta viral antigens[50], which is in line with our observations.
371 It has been well documented that spaceflight conditions impact immune cells, including a
372 reduced activity of T-cells and altered cytokine production[3,51]. This is consistent with previous
373 observations in astronauts who experienced herpesvirus reactivation during spaceflight[5-7]. Our
374 results are congruent with these observations. μG itself has a small effect in the shape of the virus
375 accumulation curve, yet increasing 2.7% the accumulated viral load along the 44 hpi period. In
376 contrast, BBR itself has a major effect in OrV accumulation dynamics, erasing the distinction
377 between both viral production phases and resulting in 34.2% reduction in accumulated viral load
378 by the end of the experiment. The result of combining both stresses fully change the temporal
379 shape of viral production, resembling the pattern observed at BBR, and further reduce the
380 accumulated viral load at the end of the experiment to 71.5%. These observations suggest that (*i*)
381 the precise simulated μG conditions may be causing a minor impairment in the nematode's
382 immune system and that (*ii*) the stress induced by BBR in nucleic acids stability impacts OrV
383 replication by a mechanism still to be found.

384 Several studies have shown that short-term exposures to μG exert small and reversible
385 alterations in the transcriptome of *C. elegans*, though prolonged expositions result in
386 transgenerational reversible effects of larger magnitude[31,52,53]. Overall, these transcriptomic
387 alterations affect longevity-regulating insulin/IGF-1[54] and sphingolipid signaling pathways[55],
388 neuronal function and/or cellular metabolism mediated by the *daf-16*/FOXO signaling pathway[56]
389 and misregulation of responses to oxidative stress and the antioxidant defense system[33]. Some of
390 these pathways have also been linked to OrV infection[54], that also often leads to the generation of
391 reactive oxygen species (ROS) as part of the immune response, creating oxidative stress[55]. In
392 principle, the failure to produce ROS antiviral responses would result in enhanced virus
393 accumulation, which we have observed in the μG conditions.

394 Our study is one of the first to explore the biological implications of the absence of muon
395 radiation flux during spaceflight on viral infection. Whilst the majority of research has focused
396 on cosmic radiation exposure or natural background radiation, the reduction of secondary cosmic
397 rays, including muons, presents an underexplored variable[29]. Furthermore, no study to our
398 knowledge has explored the effect of lack of radiation in the progression of a viral infections,
399 despite the fact that the absence of muon radiation in space could potentially contribute to the
400 observed viral activation in astronauts, with the caveat that space is composed by a complex
401 radiation environment. Muon radiation has been present during organisms' evolution as a result
402 organisms have developed mechanisms directed to cope with the effects of this type of radiation
403 in the integrity of their genetic material integrity and physiological processes. The negative
404 impact of lack of muon radiation in reproductive success aligns with the emerging theory of
405 radiation as an hormetic agent[11], in which doses below and above natural background may have
406 harmful effects for organisms. Ongoing experiments will bring to light whether the negative
407 effect of BBR on virus accumulation is a result of its impact on different cellular pathways or a
408 direct interference on viral replication.

409 The combined impact of μG and BBR, creates a singular environment that affects viral
410 infection dynamics. The results discussed above support the hypothesis that the off-Earth stresses
411 are not isolated but interact to modulate viral reactivation or replication. The immune
412 dysregulation caused by μG, when compounded by the altered radiation environment, may
413 increase the likelihood of viral outbreaks or the emergence of more virulent viral strains during
414 long-duration spaceflight. For example, the reduction in DNA repair efficiency under space
415 radiation exposure, coupled with μG-induced immune suppression, may explain the observed
416 reactivation of herpes-like viruses[5-7].

417 From our fertility modeling approach (Table 2 and discussion thereof), the observed effects
418 appear largely attributable to differences in prezygotic parameters, such as oocyte maturation and
419 fertilization rates. This aligns with earlier findings by Van Voorhies *et al*. showing that regulation

of major sperm protein genes (MSP) was altered in BBR condition[29]. MSPs were first identified as being involved in sperm motility and is required for the sperm ameboid-like crawling[56]. MSPs are also critical in other aspects of *C. elegans* reproduction, including oocyte and egg development, ovulation, spermathecal valve dilation, and parthenogenesis[57,58]. Seeing how functionally multifaceted MSPs are, it is likely that the alteration in the expression of *msp* genes in the BBR conditions may be reflected in the prezygotic parameters of the model.

In practical terms, the demonstrated relationship between altered gravity or radiation conditions and viral behavior underscores the need for enhanced monitoring and countermeasures in scenarios where gravity or radiation differ substantially from Earth's norms. Pre-flight viral screenings and vaccination strategies may need to be bolstered to mitigate the risks posed by viral reactivation. Moreover, therapeutic approaches that strengthen immune function or directly inhibit viral replication should be considered as part of space medicine protocols. Our study reinforces the importance of further research into the effects of the extraordinary spaceflight environment on viral pathogens. Understanding the precise mechanisms through which μG and radiation interact to influence viral infections will be crucial for developing comprehensive strategies to protect astronaut health span on future long-distance missions.

In conclusion, evidences presented here highlights the intricate interplay between reduced gravity, diminished muon flux and viral infection. Even introducing only a few off-Earth conditions —microgravity and below-background radiation— can substantially reshape host physiology and pathogen replication. Our findings suggest that lowered gravity may impair certain aspects of *C. elegans* immune function, allowing modest viral load increases, while the lack of muon flux alters viral accumulation dynamics in more pronounced ways. Taken together, these stressors create an environment in which viral activity and host fitness are influenced by overlapping yet distinct mechanisms. For organisms evolved in Earth's gravitational field and background radiation, deviations in these parameters —whether in orbital stations, underground conditions, or on other planetary bodies— can induce notable biological effects. Further research involving a wider range of radiation types and additional parameters will help clarify the mechanisms behind these observations and guide strategies to preserve health under non-terrestrial conditions.

METHODS

C. elegans strains and culturing

C. elegans was cultured and maintained at 20 °C on nematode growth media (NGM) agar plates seeded with *Escherichia coli* OP50. ERT54 (*jyIs8[pals-5p::GFP + myo-2p::mCherry]X*), a transgenic strain with a genetic wild-type (Bristol N2) background that expresses GFP in response

456 to intracellular infection[59] was used for all experiments. The more susceptible strain SFE2 (*drh-*
457 *1(ok3495)IV;mjls228*) was used to produce OrV stocks.
458 In order to obtain synchronized animal populations, plates with embryos were carefully
459 washed with M9 buffer to remove larvae and adults but leaving the embryos behind. Plates were
460 washed again using M9 buffer after 1 h to collect larvae hatched within that time span and
461 transferred to seeded NGM plates.
462 A variable number of plates of 500 synchronized L1 animals were used to assess male
463 frequency. Plates were stored at 20 °C and, two days after hatching, males and total population
464 were counted using a Zeiss Stemi305 stereomicroscope.
465
466 **Experimental design and locations**
467 Four different environmental conditions have been tested in this work: standard conditions, μG,
468 BBR, and the combination of μG plus BBR. Experiments conducted in standard and microgravity
469 conditions were performed in the Evolutionary Systems Virology laboratory in the Institute for
470 Integrative Systems Biology (Paterna, Spain). The experiments that included BBR conditions
471 were carried out in the Canfranc Underground Laboratory in three different periods from 2022 to
472 2024 due to technical issues.
473 μG was simulated using a RPM (Yuri Gravity GmbH) set to the zero-gravity mode. Values of
474 G-force were monitored through the RPM software and maintained at approximately 0.001 –
475 0.002 g throughout the experiments. The RPM was placed inside an incubator at 20 ºC. Animals
476 used in experiments of μG conditions were acclimated along two generations, with studies done
477 on the third generation and its progeny. Plates were sealed with parafilm to maintain their
478 humidity.
479 BBR experiments were performed in the LAB2400 at the Canfranc Underground Laboratory
480 (LSC), located in the village of Estación de Canfranc (Huesca, Spain). The measured integrated
481 muon radiation flux in this facility is ~5×10^{-3} m^{-2} s^{-1} (60). For comparison, the muon radiation
482 flux at sea level in the Northern hemisphere is about 150 m^{-2} s^{-1} (61). Thermoluminescent
483 dosimeters sensitive to various sources of radiation are placed at different locations of the
484 underground laboratory. In 2022 they showed and average dose rate of 0.71 ±0.03 mSv per year
485 in the underground facilities, compared with the 1.36 ±0.03 mSv per year of the above ground
486 laboratory[62]. Radon radiation from the mountain was reduced to 1 mBq m^{-3} thanks to a good
487 ventilation system and a Radon Abatement System, a value substantially lower than the 200–280
488 Bq m^{-3} measured at the surface laboratory[63]. Nematodes used in BBR experiments were
489 acclimated to this condition during two generations prior to experiments.
490
491 **Fertility assay**

492 L4 larvae were picked individually from a synchronized population and put in separate fresh
493 plates. Animals were transferred to fresh plates every 24 h until egg laying stopped.
494 Synchronized animal populations were inoculated after hatching. The number of nonviable (*N*)
495 and unfertilized eggs (*U*) was counted 24 h after the adult was removed from the plate to ensure
496 all eggs had hatched. Viable progeny (*A*) was counted 48 h after the adult was removed from the
497 plate. Reproductive success, *R*, was then computed as $R = A/(A + N + U)$.
498 For OrV infection experiments, a population of animals was inoculated one hour after hatching
499 with the OrV stock described below.
500
501 **Viral stock preparation, virus quantification and inoculation procedure**
502 For OrV (strain JUv1580_vlc) stock preparation, SFE2 animals were inoculated as previously
503 described[64]. In short, animals were allowed to grow for 5 days and then resuspended in M9 (0.22
504 M KH_2PO_4, 0.42 M Na_2HPO_4, 0.85 M NaCl, 0.001 M $MgSO_4$), let stand for 15 min at room
505 temperature, vortexed, and centrifuged for 2 min at 400 g. The supernatant was centrifuged twice
506 at 21,000 g for 5 min and then passed through a 0.2 μm filter. RNA of the resulting viral stock
507 was extracted using the Viral RNA Isolation kit (NZYTech). The concentration of viral RNA was
508 then determined by RT-qPCR using a standard curve, and normalized across different stocks
509 (details below). Primers used for RT-qPCRs can be found in Table S2.
510 For the standard curve, cDNA of JUv1580_vlc was obtained using AccuScript High-Fidelity
511 Reverse Transcriptase (Agilent) and reverse primers at the 3' end of the genome. Approximately
512 1000 bp of the 3' end of RNA2 were amplified using forward primers containing 20 bp coding
513 the T7 promoter and DreamTaq DNA Polymerase (Thermo Fisher). The PCR products were gel
514 purified using MSB Spin PCRapace (Invitek Molecular) and an *in vitro* transcription was
515 performed using T7 Polymerase (Merck). The remaining DNA was then degraded using DNAse
516 I (Life Technologies). RNA concentration was determined by NanoDrop (Thermo Fisher) and
517 the number of molecules per μL was determined using the online tool EndMemo RNA Copy
518 Number Calculator (https://www.endmemo.com/bio/dnacopynum.php). Primers used for the
519 standard curve can be found in Table S2.
520 For inoculation experiments, synchronized populations were inoculated by pipetting 60 μL of
521 viral stock on top of the bacterial lawn containing the animals. The normalized inoculum
522 contained $2.6 \cdot 10^7$ copies of OrV RNA2/μL. The efficiency of this viral stock (measured as
523 animals showing activation of the *pals-5p::GFP* reporter at 48 hpi) was 72 ±3 % (mean ±1 SEM,
524 $n = 5$ plates with 44 – 48 animals per plate).
525
526 **RNA extractions and RT-qPCRs**

527 Sample preparation and RNA extractions were performed as previously described[64].
528 Synchronized populations of 300 inoculated and control animals were collected at the designated
529 times (from 6 hpi to 44 hpi every 2 h) with PBS-0.05% Tween. Samples of inoculated animals
530 were performed in triplicates. Samples were centrifuged for 2 min at 1350 rpm and the
531 supernatant was discarded. Another two wash steps were performed before flash-freezing the
532 samples in liquid N_2. 500 µL of Trizol (Invitrogen) were added to the nematode pellet and the
533 pellet was disrupted by following five cycles of freeze-thawing and five cycles of 30 seconds of
534 vortex followed by 30 seconds of rest. 100 µL of chloroform were then added and the tubes were
535 shaken for 15 s and let rest for 2 min. Samples were centrifuged for 15 min at 11,000 g at 4 °C
536 and the top layer containing the RNA was then mixed with the same volume of 100% ethanol.
537 The sample was then loaded into RNA Clean & Concentrator columns (Zymo Research) and the
538 rest of the protocol was followed according to manufacturer instructions.
539 RT-qPCRs were performed using Power SYBR Green PCR Master Mix (Applied Biosystems)
540 on an ABI StepOne Plus Real-time PCR System (Applied Biosystems). 10 ng of total RNA were
541 loaded and a comparison with the endogenous gene *cdc-42* was used for relative OrV
542 quantifications. Primers used for RT-qPCRs can be found in Table S2.
543
544 **Body size measurements and analysis of abnormal phenotypes**
545 Synchronized animals were collected at 12, 24, 36, and 48 h, plates were washed with M9 buffer
546 to collect nematodes and another M9 wash was made to remove bacteria from the media. Animals
547 were mounted in a 4% agarose pad with 20% 100 mM azide and photographed using a Leica
548 Thunder DMi8 microscope with DFC9000 GTC sCMOS camera and objective HC PL APO
549 40×/0.95 CORR PH2 (Leica Microsystems). Body length was measured using the segmented
550 line tool in ImageJ[65].
551 The photographs employed to measure body size were also used to describe abnormal
552 phenotypes.
553
554 **Intestinal permeability assay**
555 The intestinal permeability assay was performed as previously described with minor
556 modifications[66]. Synchronized nematodes were washed after 48 h with S buffer (6.5 mM
557 K_2HPO_4, 43.5 mM KH_2PO_4, 100 mM NaCl) and suspended in a 1:1 solution of 1 mL of M9 buffer
558 mixed with 0.05 g of erioglaucine disodium salt (Thermo Scientific) and 1 mL of *E. coli* OP50
559 suspended in S buffer, and gently rocked for 3 h.
560 Animals were washed carefully three times with 10 mL of M9 buffer. Animals were mounted
561 on microscopic slides on top of a 4% agarose pad with 20% 100 mM azide. Photographs were
562 taken using a Leica MZ10F stereomicroscope with Flexacam C3 camera and with a Leica DMi1
563 microscope with Flexacam C1 camera. Quantifications were randomized by assigning random

names to photographs to avoid observer bias. A positive control was prepared to help us to classify the different phenotypes. Positive control was prepared by following the same assay except that animals were grown in NGM plates with 0.8 mM H_2O_2 during 48 h, as previously described[67]. Four-hundred nematodes were used in each condition.

A model of *C. elegans* fecundity and parameter estimation

Figure 5 describes a simple fecundity model for sexually mature adults at L4 developmental stage, in which a fixed number of spermatocyte cells (S) have already been produced and stored in the spermathecae. Germline precursor cells (G) differentiate into mature oocytes (O) at rate δ_G. This rate is assumed to be constant $\delta_G = \delta$ as far as germline cells exist ($G(t) > 0$) and zero otherwise. These oocytes migrate from the distal to the proximal gonads at rate η until reaching the spermathecae where, if spermatocytes are available, are fecundated with an efficiency function ψ that depends on the amount of S present in the spermatheca at time t: $\psi(S) = (1-\gamma)S/(\gamma + S) \in [0,1]$, where γ is a dimensionless parameter which modulates the value of the efficiency, resulting in fertilized and unfertilized (U) eggs. After passing through the uterus, the eggs are deposited in the agar, where, if they have been fecundated, a fraction μ will develop into L1 larvae (*i.e*, the viable progeny, A). A fraction $1 - \mu$ will stop embryonic development, resulting in nonviable embryos (N). N and U eggs will simply remain in the plates and are easily distinguishable.

Parameter	Description
δ_G	Rate of germline precursor cells differentiation
η	Rate of oocytes migration
Ψ	Fertilization efficiency
μ	Fraction of fertilized eggs viability
α	Spermatocytes to germline initial ratio

Variable	Description
G	Germline precursor cells
O	Oocytes
S	Spermatocytes
U	Unfertilized eggs
A	Viable progeny
N	Non-viable eggs

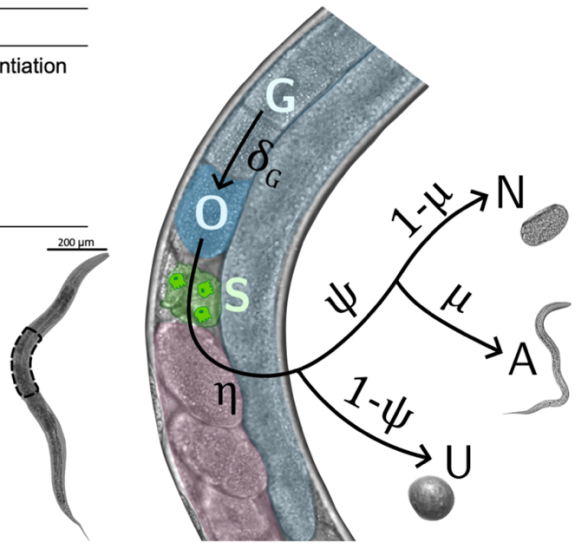

Figure 5. Parameters, variables and schematic representation of the fecundity model described by Eq. 1 – 6.

These processes can be written according to the following set of ordinary differential equations,

$$\frac{dG}{dt} = -\delta_G, \quad \text{Eq. 1}$$

$$\frac{dO}{dt} = \delta_G - \eta O, \quad \text{Eq. 2}$$

$$\frac{dS}{dt} = -\eta\psi O, \quad \text{Eq. 3}$$

$$\frac{dA}{dt} = \eta\mu\psi O, \quad \text{Eq. 4}$$

$$\frac{dN}{dt} = \eta(1-\mu)\psi O, \text{and} \quad \text{Eq. 5}$$

$$\frac{dU}{dt} = \eta(1-\psi)O, \quad \text{Eq. 6}$$

being A, N, and U are the three experimental observables (Eqs. 4 – 6). All variables were normalized by the initial number of non-differentiated germinal cells G_0. Model parameters δ, η and γ represent prezygotic stages, while μ represents a postzygotic event. Furthermore, we define the dimensionless parameter $\alpha = S_0/G_0$, which for a hermaphrodite in which the spermatocytes will be the limiting factor for asexual reproduction will be $\alpha < 1$.

We used a genetic algorithm to estimate the vector of parameters (δ, η, μ, γ, α, G_0) better fitting the experimental data for every condition. The size of the population of vectors of parameters was fixed at 600, and the number of generations was set to 10^4. The exploration of the parameter space was refined through successive generations. The cost function ($\mathcal{F}$) to minimize was the logarithm of the square sum of discrepancies:

$$\mathcal{F} = \log \sum_{i=1}^{T} \left[\left(A_i - \hat{A}_i\right)^2 + \left(N_i - \widehat{N}_i\right)^2 + \left(U_i - \widehat{U}_i\right)^2 \right]. \quad \text{Eq. 7}$$

Here, $\{t_i, A_i, N_i, U_i\}_{i=1}^{T}$ represent the experimental data obtained for T different times and $\hat{A}_i$, $\widehat{N}_i$ and $\widehat{U}_i$ denote the estimated values for the different species obtained with the mathematical model for a given set of parameters.

Within each generation, the 5% of the parameters with the lowest $\mathcal{F}$ values were designated as the elite population, remaining constant for the next generation. The next-best 80% underwent parameter crossover, while the remaining 15%, representing the least favorable parameters, experienced random mutations. The parameter space was subdivided into a logarithmic scale for parameters δ, η and γ to ensure a more balanced exploration. The model was fitted to every fertility assay data, resulting in a vector of estimated parameters per experimental replicate and condition.

Statistical analyses

Data were fitted to generalized linear mixed models (GLMM) with gravity intensity (standard *vs* μG), radiation level (standard *vs* BBR) and infection status (non-inoculated *vs* inoculated)

incorporated as fixed orthogonal factors, whereas individual animals (subjects) and days-post inoculation (repeated measures per subject) were both modeled as random factors. In the case of counts (*A*, *N* and *U*), a Poisson distribution with a log-link function was used; in the case of *R* and body size, a Normal distribution with identity-link function was used.

Intestinal permeability and the frequency of males per population data were fitted to logistic regression models using generalized linear models (GLM) with gravity intensity and radiation level incorporated as fixed orthogonal factors and assuming a Binomial distribution and a logit-link function.

Viral load data were fitted to a GLMM with gravity intensity and radiation level incorporated as fixed orthogonal factors, whereas replicate plates (subjects) and hpi (repeated measures per subject) were both modeled as random factors, a Gamma distribution with a log-link function was used.

Estimated parameters of the model described by Eqs. 1 – 6 were independently fitted to ANOVA models with gravity intensity, radiation level and infection status incorporated as fixed orthogonal factors. Errors were assumed to be Normal.

In all cases, pairwise *post hoc* comparisons were done with the sequential Bonferroni method. The magnitude of the effects was calculated using the η_P^2 statistic, *i.e.*, the proportion of variance in the dependent variable that can be attributed to each model factor after accounting for the variance explained by other factors in the model. Typically, values of $0.06 \leq \eta_P^2 < 0.15$ are considered as medium size effects and $\eta_P^2 \geq 0.15$ are as large magnitude effects.

These analyses were done with SPSS version 29.0.2.0 (IBM Corporation, Armonk, NY)

DATA AVAILABILITY

The datasets generated during the current study are available in the Zenodo respository, https://doi.org/10.5281/zenodo.13869555.

REFERENCES

1. Crucian, B. *et al*. Immune system dysregulation occurs during short duration spaceflight on board the space shuttle. *Journal of Clinical Immunology* **33**, 456–465 (2013).
2. Crucian, B. *et al*. Alterations in adaptive immunity persist during long-duration spaceflight. *npj Microgravity* **1**, 15013 (2015).
3. Bigley, A. B. *et al.* NK cell function is impaired during long-duration spaceflight. *Journal of Applied Physiology* **126**, 842–853 (2019).
4. Agha, N. H. *et al*. Salivary antimicrobial proteins and stress biomarkers are elevated during a 6-month mission to the International Space Station. *Journal of Applied Physiology* **128**, 264–

275 (2020).

5. Rooney, B. V. B., Crucian, B. E., Pierson, D. L., Laudenslager, M. L. & Mehta, S. K. Herpes virus reactivation in astronauts during spaceflight and its application on Earth. *Frontiers in Microbiology* **10**, 16 (2019).
6. Mehta, S. K. *et al*. Multiple latent viruses reactivate in astronauts during Space Shuttle missions. *Brain Behavior and Immunity* **41**, 210–217 (2014).
7. Mehta, S. K. *et al*. Latent virus reactivation in astronauts on the international space station. *npj Microgravity* **3**, 11 (2017).
8. Bonomi, G., Checchia, P., D'Errico, M., Pagano, D. & Saracino, G. Applications of cosmic-ray muons. *Progress in Particle and Nuclear Physics* **112**, 103768 (2020).
9. Zhao, L. *et al.* The determinant of DNA repair pathway choices in ionizing radiation-induced DNA double-strand breaks. *BMC Research International* **2020**, 4834965 (2020).
10. Ceccaldi, R., Rondinelli, B. & D'Andrea, A. D. Repair pathway choices and consequences at the double-strand break. *Trends in Cell Biology* **26**, 52–64.
11. Baldwin, J. & Grantham, V. Radiation hormesis: historical and current perspectives. *Journal of Nuclear Medicine Technology* **43**, 242–246 (2015).
12. Brenner, S. The genetics of *Caenorhabditis elegans*. *Genetics* **77**, 71–94 (1974).
13. Kim, W., Underwood, R. S., Greenwald, I. & Shaye, D. D. OrthoList 2: A New comparative genomic analysis of human and *Caenorhabditis elegans* genes. *Genetics* **210**, 445–461 (2018).
14. Olsen, A., Vantipalli, M. C. & Lithgow, G. J. Lifespan extension of *Caenorhabditis elegans* following repeated mild hormetic heat treatments. *Biogerontology* **7**, 221–230 (2006).
15. Aprison, E. Z. & Ruvinsky, I. Balanced trade-offs between alternative strategies shape the response of *C. elegans* reproduction to chronic heat stress. *PLoS ONE* **9**, e105513 (2014).
16. Begasse, M. L., Leaver, M., Vazquez, F., Grill, S. W. & Hyman, A. A. Temperature dependence of cell division timing accounts for a shift in the thermal limits of *C. elegans* and *C. briggsae*. *Cell Reports* **10**, 647–653 (2015).
17. Rodriguez, M., Snoek, L. B., Riksen, J. A. G., Bevers, R. P. & Kammenga, J. E. Genetic variation for stress-response hormesis in *C. elegans* lifespan. *Experimental Gerontology* **47**, 581–587 (2012).
18. Jovic, K. *et al*. Temporal dynamics of gene expression in heat-stressed *Caenorhabditis elegans*. *PLoS ONE* **12**, e0189445 (2017).
19. Rohlfing, A.K., Miteva, Y., Hannenhalli, S. & Lamitina, T. Genetic and physiological activation of osmosensitive gene expression mimics transcriptional signatures of pathogen infection in *C. elegans*. *PLoS ONE* **5**, e9010 (2010).
20. Prithika, U., Deepa, V. & Balamurugan, K. External induction of heat shock stimulates the immune response and longevity of *Caenorhabditis elegans* towards pathogen exposure. *Innate Immunity* **22**, 466–478 (2016).

21. Leroy, M., Mosser, T., Manière, X., Alvarez, D. F. & Matic, I. Pathogen-induced *Caenorhabditis elegans* developmental plasticity has a hormetic effect on the resistance to biotic and abiotic stresses. *BMC Evolutionary Biology* **12**, 187 (2012).
22. Castiglioni, V. G. & Elena, S. F. Orsay virus infection increases *Caenorhabditis elegans* resistance to heat-shock. *Biology Letters* **20**, 20240278 (2024).
23. Panek, J. *et al*. A cullin-RING ubiquitin ligase promotes thermotolerance as part of the intracellular pathogen response in *Caenorhabditis elegans*. *Proceedings of the National Academy of Sciences of the USA* **117**, 7950–7960 (2020).
24. De Souza, E. A., Thompson, M. A. & Taylor, R. C. Olfactory chemosensation extends lifespan through TGF-β signaling and UPR activation. *Nature Aging* **3**, 938–947 (2023).
25. Le Pen, J. *et al*. Terminal uridylyltransferases target RNA viruses as part of the innate immune system. *Nature Structural Molecular Biology* **25**, 778–786.
26. Ashe, A. *et al*. A deletion polymorphism in the *Caenorhabditis elegans* RIG-I homolog disables viral RNA dicing and antiviral immunity. *eLife* **2**, e00994 (2013).
27. Félix, M.A. *et al*. Natural and experimental infection of *Caenorhabditis* nematodes by novel viruses related to nodaviruses. *PLoS Biology* **9**, e1000586 (2011).
28. Huang, Y. *et al*. Heat stress reduces the susceptibility of *Caenorhabditis elegans* to Orsay virus infection. *Genes* **12**, 1161 (2021).
29. Van Voorhies, W. A., Castillo, H. A., Thawng, C. N. & Smith, G. B. The phenotypic and transcriptomic response of the *Caenorhabditis elegans* nematode to background and below-background radiation levels. *Frontiers in Public Health* **8**, 581796 (2020).
30. Morciano, P. *et al*. Effects of reduced natural background radiation on *Drosophila melanogaster* growth and development as revealed by the FLYINGLOW program. *Journal of Cellular Physiology* **233**, 23–29 (2018).
31. Tee, L. F. *et al.* Effects of simulated microgravity on gene expression and biological phenotypes of a single generation *Caenorhabditis elegans* cultured on 2 different media. *Life Sciences in Space Research* **15**, 11–17 (2017).
32. Liu, H., Guo, D., Kong, Y., Rui, Q. & Wang, D. Damage on functional state of intestinal barrier by microgravity stress in nematode *Caenorhabditis elegans*. *Ecotoxicology and Environmental Safety* **183**, 109554 (2019).
33. Zhao, L., Rui, Q. & Wang, D. Molecular basis for oxidative stress induced by simulated microgravity in nematode *Caenorhabditis elegans*. *Science of the Total Environment* **607–608**, 1381–1390 (2017).
34. Zhou, Y., Chen, H., Zhong, W. & Tao, Y. J. Collagen and actin network mediate antiviral immunity against Orsay virus in *C. elegans* intestinal cells. *PLoS Pathogens* **20**, e1011366 (2024).
35. Martel, J. *et al.* Gut barrier disruption and chronic disease. *Trends in Endocrinology &*

721 *Metabolism* **33**, 247–265 (2022).
722 36. Castiglioni, V. G. *et al*. Story of an infection: viral dynamics and host responses in the
723 *Caenorhabditis elegans*-Orsay virus pathosystem. *Science Advances* **10**, eadn5945 (2024).
724 37. Félix, M. A. & Wang, D. Natural viruses of *Caenorhabditis* nematodes. *Annual Review of*
725 *Genetics* **53**, 313–326 (2019).
726 38. Morran, L. T., Cappy, B. J., Anderson, J. L. & Phillips, P. C. Sexual partners for the stressed:
727 facultative outcrossing in the self-fertilizing nematode *Caenorhabditis elegans*. *Evolution* **63**,
728 1473–1482 (2009).
729 39. Johnstone, I. L. Cuticle collagen genes. Expression in *Caenorhabditis elegans*. *Trends in*
730 *Genetics* **16**, 21–27 (2000).
731 40. Hicks, J., Olson, M., Mitchell, C., Juran, C. M. & Paul, A. M. The impact of microgravity on
732 immunological states. *Immunohorizons* **7**, 670–682 (2023).
733 41. Shearer, W. T., Zhang, S., Reuben, J. M., Lee, B. N. & Butel, J. S. Effects of radiation and
734 latent virus on immune responses in a space flight model. *Journal of Allergy and Clinical*
735 *Immunology* **115**, 1297–1303 (2005).
736 42. Chancellor, J. C. *et al.* Limitations in predicting the space radiation health risk for exploration
737 astronauts. *npj Microgravity* **4**, 8 (2018).
738 43. Adenle, A. A., Johnsen, B. & Szewczyk, N. J. Review of the results from the International *C.*
739 *elegans* first experiment (ICE-FIRST). *Advances in Space Research* **44**, 210–2016 (2009).
740 44. Wuest, S. L., Stern, P., Casartelli, E. & Egli, M. Fluid dynamics appearing during simulated
741 microgravity using random positioning machines. *PLoS ONE* **12**, e0170826 (2017).
742 45. Çelen, I., Doh, J. H. & Sabanayagam, C. R. Effect of liquid cultivation on gene expression and
743 phenotype of *C. elegans*. *BMC Genomics* **19**, 562 (2018).
744 46. Lev, I., Bril, R., Liu, Y., Ceré, L. I. & Rechavi, O. Inter-generational consequences for growing
745 *Caenorhabditis elegans* in liquid. *Philosophical Transactions of the Royal Society B:*
746 *Biological Sciences* **374**, 20180125 (2019).
747 47. Goswami, P. C., Roti Roti, J. L. & Hunt, C. R. The cell cycle-couple expression of
748 topoisomerase IIα during S phase is regulated by mRNA stability and is disrupted by heat
749 shock or ionizing radiation. *Molecular and Cellular Biology* **16**, 1500-1508 (1996).
750 48. Slowinski, S. P. *et al*. Outcrossing in *Caenorhabditis elegans* increases in response to food
751 limitation. *Ecology and Evolution* **14**, e11166 (2024).
752 49. Higashibata, A. *et al*. Microgravity elicits reproducible alterations in cytoskeletal and
753 metabolic gene and protein expression in space-flown *Caenorhabditis elegans*. *npj*
754 *Microgravity* **2**, 15022 (2016).
755 50. Lee, L. W., Chang, T. Y., Lo, H. W. & Lo, S. J. Hepatitis D antigens cause growth retardation
756 and brood-size reduction in *C. elegans*. *Frontiers in Biosciences* **3**, 380–390 (2011).
757 51. Lv, H. *et al*. Microgravity and immune cells. *Journal of the Royal Society Interface* **20**,

758 20220869 (2023).
759 52. Willis, C. R. G. *et al*. Comparative transcriptomics identifies neuronal and metabolic
760 adaptations to hypergravity and microgravity in *Caenorhabditis elegans. iScience* **23**, 101734
761 (2020).
762 53. Çelen, I., Jayasinghe, A., Doh, J. H. & Sabanayagam, C. R. Transcriptomic signature of the
763 simulated microgravity response in *Caenorhabditis elegans* and comparison to spaceflight
764 experiments. *Cells* **12**, 270 (2023).
765 54. Duxbury, E. M. L. *et al*. Reduced insulin/IGF-1 signaling upregulates two anti-viral immune
766 pathways, decreases viral load and increases survival under viral infection in *C. elegans*.
767 *GeroScience* https://doi.org/10.1007/s11357-024-01147-7 (2024).
768 55. Van der Hoeven, R., McCallum, K. C., Cruz, M. R. & Garsin, D. A. Ce-Duox1/BLI-3
769 generated reactive oxygen species trigger protective SKN-1 activity via p39 MAPK signaling
770 during infection in *C. elegans*. *PLoS Pathogens* **7**, e1002453 (2011).
771 56. L'Hernault, W. E. Spermatogenesis. In: Riddle, D. L. (ed). *C. elegans II*. Cold Spring Harbor,
772 NY: Cold Spring Harbor Laboratory Press (1997). pp. 271-94.
773 57. McGovern, M., Yu, L., Kosinski, M., Greenstein, D. & Savage-Dunn, C. A role for sperm in
774 regulation of egg-laying in the nematode *C. elegans*. *BMC Developmental Biology* **7**, 41
775 (2007).
776 58. Kuwabara, P. E. The multifaceted *C. elegans* major sperm protein: an ephrin signaling
777 antagonist in oocyte maturation. *Genes Development* **17**, 155-161 (2003).
778 59. Bakowski, M. A. *et al.* Ubiquitin-mediated response to microsporidia and virus infection in *C.*
779 *elegans*. *PLoS Pathogens* **10**, e1004200 (2014).
780 60. Trzaska, W. H., *et al*. Cosmic-ray muon flux at Canfranc Underground Laboratory. *European*
781 *Physical Journal C* **79**, 721 (2019).
782 61. Workman, R. L. *et al*. The review of particle physics. *Progress in Theoretical and*
783 *Experimental Physics* **2022**, 083C01 (2022).
784 62. Hernández-Antolín, R., Cid-Barrio, L. & Peña-Garay, C. Canfranc biology platform: exploring
785 life in cosmic silence. *Frontiers in Physics* **12**, 1397799 (2024).
786 63. Pérez-Pérez, J. *et al.* Radon mitigation applications at the Laboratorio Subterráneo de Canfranc
787 (LSC). *Universe* **8**, 112 (2022).
788 64. Castiglioni, V. G., *et al*. Experimental evolution of an RNA virus in *Caenorhabditis elegans*.
789 *Infection Genetics and Evolution* **123**, 105623 (2024).
790 65. Schindelin, J., *et al*. Fiji: an open-source platform for biological-image analysis. *Nature*
791 *Methods* **9**, 676-682 (2012).
792 66. Kissoyan, K. A. B., *et al.* Natural *C. elegans* microbiota protects against infection via
793 production of a cyclic lipopeptide of the viscosin group. *Current Biology* **29**, 1030-1037.e5
794 (2019).

67. Balaguer, F., *et al*. *Bifidobacterium animalis* subsp. *lactis* BPL1™ and its lipoteichoic acid modulate longevity and improve age/stress-related behaviors in *Caenorhabditis elegans*. *Antioxidants* **12**, 2107 (2023).

ACKNOWLEDGEMENTS

We thank Francisca de la Iglesia (I2SysBio) and Rebecca Hernández-Antolín (LSC) for excellent technical support. We are deeply grateful to Carlos Peña-Garay (LSC) for his commitment and dedication to research in subterranean biology, as well as his constant material and emotional support. Many computations were performed on the HPC cluster Garnatxa at I2SysBio (CSIC-UV). This study was supported by ESA contract 4000135960/21/NL/GLC/my, grant PID2022-136912NB-I00 funded by MCIN/AEI/10.13039/501100011033 and by "ERDF a way of making Europe", grant CIPROM/2022/59 funded by Generalitat Valenciana, and grant PB-02-22 from ICTS Laboratorio Subterráneo de Canfranc to S.F.E. V.G.C. was supported by grant FJC2021-047264-I funded by MCIN/AEI/10.13039/501100011033 and by NextGenerationEU/PRTR. E.G.L. was supported by grant FPU21/00410 funded by MCIN/AEI/10.13039/501100011033 and by "ESF invest in your future". J.C.M-S. was supported by grant ACIF/2021/296 from Generalitat Valenciana. The funders played no role in study design, data collection, analysis and interpretation of data, or the writing of this manuscript.

AUTHOR CONTRIBUTIONS

AVG, VGC and EGL performed the experiments; VGC and SFE supervised the experimental work; AVG, RG, VGC, and SFE conceived and designed the experiments; AVG, JCMS and SFE analyzed the data; JCMS and SFE developed the mathematical model; AVG and SFE wrote the paper; AVG, VGC, JCMS, EGL, RG, and SFE edited and approved the final version.

COMPETING INTERESTS

The authors declare no financial or non-financial competing interests.

ADDITIONAL INFORMATION

Supplementary information The online version contains supplementary material available at https://doi.org/.

Correspondence and requests for materials should be addressed to Santiago F. Elena.

Table 1. Results of the fecundity data fitting to the GLMM testing for the effect of gravity intensity, muon radiation flux and OrV infection. Significant effects of small magnitude are highlighted in light gray, while significant effects of medium and large magnitude are highlighted in dark gray.

		Unfertilized eggs (*U*)			**Nonviable embryos (*N*)**			**Progeny (*A*)**			**Reproductive success (*R*)**		
Source of variation	**d.f.**	F	P	η_P^2	F	P	η_P^2	F	P	η_P^2	F	P	η_P^2
Model	7, 592	3.113	0.003	0.036	11.702	< 0.001	0.122	13.129	< 0.001	0.134	19.737	< 0.001	0.189
Gravity intensity	1, 592	1.923	0.166	0.003	3.825	0.051	0.006	22.538	< 0.001	0.037	13.221	< 0.001	0.022
Muon radiation flux	1, 592	1.122	0.290	0.002	5.010	0.026	0.008	0.410	0.522	0.001	0.425	0.515	0.001
Infection status	1, 592	3.864	0.050	0.006	9.244	0.002	0.015	19.131	< 0.001	0.031	47.457	< 0.001	0.074
Gravity × Radiation	1, 592	1.866	0.172	0.003	23.054	< 0.001	0.037	21.024	< 0.001	0.034	9.599	0.002	0.016
Gravity × Infection	1, 592	1.968	0.161	0.003	12.585	< 0.001	0.021	13.209	< 0.001	0.022	14.810	< 0.001	0.024
Radiation × Infection	1, 592	1.624	0.203	0.003	15.129	< 0.001	0.025	1.097	0.295	0.002	8.321	0.004	0.014
Gravity × Radiation × Infection	1, 592	2.020	0.156	0.003	0.259	0.611	0.000	6.689	0.010	0.011	10.964	< 0.001	0.018

Table 2. Estimation of model parameters and initial condition. Values represent the mean of the replicates (±1 SD). See Fig. S2 for the fitting to the experimental data.

Gravity intensity	Muon radiation flux	Infection status	G_0	α	δ (d^{-1})	η (d^{-1})	γ	μ
Standard	Standard	non-inoculated	252.773 ±32.217	0.936 ±0.011	0.891 ±0.215	0.584 ±0.235	0.015 ±0.011	0.989 ±0.003
Standard	Standard	inoculated	303.236 ±113.438	0.912 ±0.129	0.543 ±0.126	1.199 ±0.497	0.004 ±0.005	0.988 ±0.005
μG	Standard	non-inoculated	277.392 ±21.302	0.938 ±0.049	0.667 ±0.166	0.659 ±0.103	0.004 ±0.003	0.986 ±0.014
μG	Standard	inoculated	292.661 ±84.967	0.824 ±0.100	0.486 ±0.138	1.242 ±0.329	0.029 ±0.036	0.970 ±0.028
Standard	BBR	non-inoculated	293.401 ±27.615	0.924 ±0.068	0.416 ±0.072	0.676 ±0.220	0.013 ±0.020	0.974 ±0.008
Standard	BBR	inoculated	356.747 ±66.461	0.844 ±0.105	0.417 ±0.075	0.764 ±0.282	0.019 ±0.019	0.983 ±0.012
μG	BBR	non-inoculated	257.598 ±65.897	0.888 ±0.095	0.495 ±0.084	0.689 ±0.438	0.012 ±0.018	0.978 ±0.015
μG	BBR	inoculated	283.136 ±57.662	0.853 ±0.103	0.451 ±0.128	0.641 ±0.197	0.028 ±0.033	0.975 ±0.014

G_0: Germline precursor cells at $t = 0$; α: germline precursor cells to spermatocytes initial ratio; δ: rate of germline precursor cells differentiation into mature oocytes; η: rate of oocytes migration from the distal gonads to the spermathecae; γ: scale parameter of the fecundation efficiency function; μ: fraction of a fecundated eggs developing into an L1 larvae ($1 - \mu$ would be the fraction of a fecundated eggs which abort its development).

835